Journal of Receptors and Signal Transduction

http://informahealthcare.com/rst
ISSN: 1079-9893 (print), 1532-4281 (electronic)

J Recept Signal Transduct Res, Early Online: 1–11
 DOI: 10.3109/10799893.2014.984310

informa
healthcare

RESEARCH ARTICLE

Dynamic features of apo and bound HIV-Nef protein reveal the anti-HIV dimerization inhibition mechanism

Suri Moonsamy*, Soumendranath Bhakat*, and Mahmoud E. S. Soliman

School of Health Sciences, University of KwaZulu-Natal, Durban, South Africa

Abstract

The first account on the dynamic features of Nef or negative factor, a small myristoylated protein located in the cytoplasm believes to increase HIV-1 viral titer level, is reported herein. Due to its major role in HIV-1 pathogenicity, Nef protein is considered an emerging target in anti-HIV drug design and discovery process. In this study, comparative long-range all-atom molecular dynamics simulations were employed for apo and bound protein to unveil molecular mechanism of HIV-Nef dimerization and inhibition. Results clearly revealed that B9, a newly discovered Nef inhibitor, binds at the dimeric interface of Nef protein and caused significant separation between orthogonally opposed residues, namely Asp108, Leu112 and Gln104. Large differences in magnitudes were observed in the radius of gyration (~1.5 Å), per-residue fluctuation (~2 Å), C-alpha deviations (~2 Å) which confirm a comparatively more flexible nature of apo conformation due to rapid dimeric association. Compared to the bound conformer, a more globally correlated motion in case of apo structure of HIV-Nef confirms the process of dimeric association. This clearly highlights the process of inhibition as a result of ligand binding. The difference in principal component analysis (PCA) scatter plot and per-residue mobility plot across first two normal modes further justifies the same findings. The in-depth dynamic analyses of Nef protein presented in this report would serve crucial in understanding its function and inhibition mechanisms. Information on inhibitor binding mode would also assist in designing of potential inhibitors against this important HIV target.

Keywords

B9, HIV-Nef; dimerization, molecular dynamics

History

Received 19 September 2014
Revised 30 October 2014
Accepted 2 November 2014
Published online 19 November 2014

Introduction

Since its emergence in early 1980s, the ''global killer'' acquired immunodeficiency syndrome (AIDS) has already proclaimed the lives of estimated 22 million people worldwide (1). To date, the human immunodeficiency virus type 1 (HIV-1), the instrumental agent in causing AIDS, is regarded as one the most challenging epidemic in the history of infectious diseases (1,2). According to different documented reports, an estimated 34 million individuals live with HIV/AIDS world-wide (3,4). Let alone in sub-Saharan Africa, an approximated 22.9 million individuals constitute the overall global estimate (3,4). Despite the continuous global effort, no cure yet exists for HIV/AIDS. Currently, the most effective therapeutic regimes consists of a multiple drug ''cocktail'', otherwise known as highly active antiretroviral therapy (HAART), approved by the Food and Drug Administration (FDA), which consists of several antiretroviral, targeting different enzymes in HIV life cycle (5). These drugs mainly include: protease inhibitors (PIs), integrase (IN) inhibitors reverse transcriptase (RT) inhibitors, entry inhibitors and progression inhibitors (6).

The development of resistant strains against almost all currently approved anti-retrovirals prompt researchers to find new drug targets, which can prove effective in reducing viral load from the host. The recently discovered HIV-Nef target, a small 27–35 kDa myristoylated protein, which plays a major role in HIV-1 pathogenicity (7). Nef localizes primarily in the cytoplasm, but also partially to the plasma membrane and is one of many pathogen-expressed proteins, known as virulence factors. When undergoes dimerization in HIV, Nef protein is able to manipulate the host's cellular machinery and thus allow infection, survival or replication of the pathogen (8). Nef stands for ''Negative Factor'' and even though the viral protein is a major component for HIV-1 replication in infected hosts, Nef markedly elevates viral titers (4). As Nef is one of the accessory proteins of the HIV genome, it has a central role in the down-regulation of host immunity.

Because of its major role in HIV-1 pathogenicity, Nef protein has been proved to be a very important target in anti-HIV drug design and discovery process. Understanding Nef dimerization process and its inhibition mechanism is crucial for the design of potent inhibitors as anti-HIV. To date, a handful of small molecule inhibitors were identified using

*Both authors contributed equally to this work.

Address for correspondence: Dr Mahmoud E. S. Soliman, PhD, School of Health Sciences, University of KwaZulu-Natal, Westville Campus, Durban 4001, South Africa. Tel: +27 031 260 7413. Fax: +27 031 260 779. E-mail: soliman@ukzn.ac.za

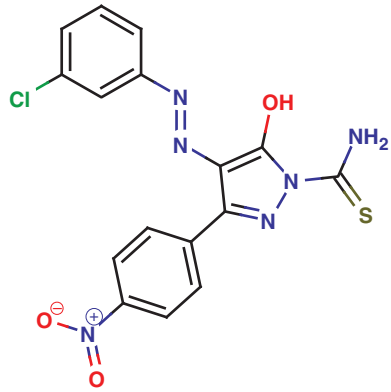

Figure 1. Two-dimensional structural representation of diphenylpyrazolodiazene containing Nef inhibitor, B9.

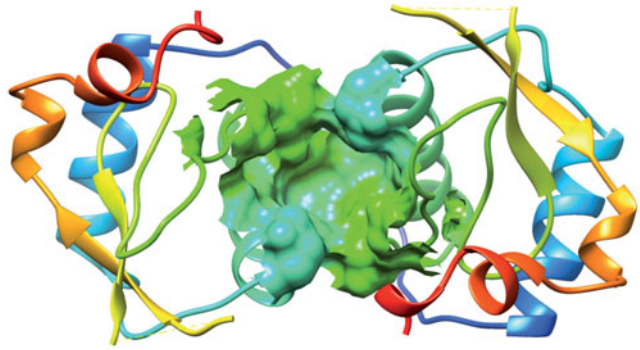

Figure 2. Graphical representation of HIV-Nef active site located at the junction of dimeric cleavage.

high throughput screening (HTS), which block the Nef-dependent HIV replication. Among them, a diphenylpyrazolodiazene containing small molecule inhibitor, B9 (Figure 1) appeared to be specifically potent (IC50 2.8 μm) at blocking Nef activity by preventing dimerization of the two Nef subunits (9,10). The binding pocket of compound B9 with HIV-Nef dimeric interface proved as a future ''hot spot'' to target this protein (9).

Molecular dynamics simulations and post-dynamics calculations emerged as a close counterpart to experiment and helps in understanding the complex biological phenomenas. Application of long-range molecular dynamics simulations to unveil folding-unfolding behavior of biological macromolecules paved a way to understand the complex process of macromolecular dimerization (11–15). Recent applications of enhanced post-dynamics approaches proved to be efficient in understanding the conformational landscape of biological macromolecules. Principal component analysis (PCA) or essential dynamics analysis is one of the widely used enhanced post-dynamics approaches to explore structural fluctuations among different biological systems (6,16). A large portion of overall fluctuation can often be accounted by a few low frequency eigenvectors with high Eigen values. If motion between two different macromolecules is similar then the Eigen vectors coming from individual trajectories should be similar to each other. For this reason, PCA has proved to be an efficient tool that can be used to compare motions of different macromolecules. Besides principal component analysis a number of post-dynamics analyses were also applied to understand the conformational behavior of biological systems (6,17–24). Dynamic cross-correlation analysis is one of those techniques, which has been applied to understand the difference in macromolecular motion across different biological systems (25,26).

In order to understand the dynamic landscape HIV-Nef dimerization process and its inhibition, comparative molecular dynamics simulations were employed for the apo and bound protein. A wide range of post-dynamic analyses were carried out in order to accomplish this task – these include, dynamic cross correlation (DCC), principal component analysis (PCA), radius of gyration (Rg), protein mobility plots as well as monitoring other several metrics.

To the best of our knowledge, this is the first account of such comprehensive computational study on this crucial HIV target. Therefore, we believe that this report serves as a cornerstone towards the understanding HIV-Nef protein structure and dynamics and its inhibitory mechanism. The compilation of computational and bioinformatics tools presented herein could also be implemented within the drug discovery and development of more potent HIV inhibitors against Nef.

Computational methods

Protein structure preparation

The crystal structure of HIV–Nef conserved core in complex with SH3 domain was retrieved from protein data bank (PDB: 1EFN) for subsequent simulations (27). The SH3 domain was deleted from the protein system to generate a native model of HIV-Nef core domain. The protein structure was prepared using Chimera's (28) molecular modeling suite.

B9-Nef complex preparation

The recent diphenylpyrazole-based HIV-Nef inhibitor, B9, was believed to bind at dimeric region of HIV-Nef (9). To generate an initial starting structure of B9-Nef complex, B9 was docked into the active site of HIV-Nef, which is located at the helical dimeric region (9,10) of HIV-Nef (Figure 2). Prior to docking, the ligand and protein systems were prepared as explained in our previous reports (29,30). Autodock Vina (31) was used to generate docked conformations of B9-HIV-Nef complex.

The active site of HIV-Nef conserved domain is highlighted in Figure 2 and Table 1 and was used to generate a grid box with a spacing set at 1 Å and an exhaustiveness of 8. The top docked conformation of compound B9 complexed with HIV-Nef was then visualized using ViewDock plugin (32) integrated with Chimera (28).

Molecular dynamic simulations

All-atom explicit solvation molecular dynamics simulations were performed on both apo and B9 bound conformations of HIV-Nef using Amber12 (6,33). The GPU version of PMEMD engine provided with Amber 12 was used to perform all molecular dynamics simulations. The restrained electrostatic potential (RESP) procedure was used to generate atomic partial charges and geometry was optimized using Gaussian 09 at the HF/6-31G* level (14). The ANTECHAMBER module

Table 1. The active site residues and GRID box dimensions used to dock compound, B9 inside HIV-Nef active site.

Protein System	Active site residues*	Grid box dimensions
HIV-Nef conserved core domain	Gln104B, Gln107B, Asp108B	Number of points
	Asp111B, Leu112B, Pro122B	$X = 22.0$ Å
	Asp123B, Trp124B, Gln125B	$Y = 24.0$ Å
	Asn126B, Gln104D	$Z = 24.0$ Å
	Gln107D, Asp108D	Centre Grid Box
	Asp111D, Pro122D	$X = 44.0$ Å
	Asp123D, Trp124D	$Y = 18.0$ Å
	Gln125D, Asn126D	$Z = 37.0$ Å

*B and D refers to dimeric chains of HIV-Nef conserved core domain.

was used to generate atomic partial charges for the ligand using GAFF force field (34). The ff99sb force field implemented with Amber 12 was used to describe the protein system (35). The LEAP module integrated with Amber 12 was used to add missing hydrogens and heavy atoms and required counter ions to neutralize the system. To ensure the correct protonation state of individual amino acids, the Leap-generated receptor structure is compared with receptor structures generated by H++ (http://biophysics.cs.vt.edu/H++) at different pH (see Supplementary Informations). Both the systems were immersed into an orthorhombic box with TIP3P (36) water molecules, such that no atom was within 10 Å of any box edge. Periodic boundary conditions were enforced and long-range electrostatic interactions were treated using particle mesh Ewald (PME) method (37) with a direct space and vdW cut-off 12 Å. Prior to system preparations, the minimizations, heating and equilibration steps were performed as described in our recent report (6). Finally, a 100 ns production run was performed in a isothermal-isobaric ensemble (NPT) ensemble with target pressure of 1 bar and a coupling constant of 2 ps.

The trajectory in both cases were saved and analyzed in every 1 ps. The PTRAJ and CPPTRAJ modules (38) integrated with Amber 12 were used for post-MD analysis, e.g. RMSD, RMSF, Rg, distance, PCA. All visualizations and plots were carried out using Chimera (28)/VMD (39) and Origin data analysis tool, respectively.

Dynamic cross correlation

The dynamic cross correlation between the residue-based fluctuations during simulation was calculated using the CPPTRAJ module integrated with Amber 12. The following equation describes the DCCR as:

$$C_{ij} = \frac{\langle \Delta r_i \cdot \Delta r_j \rangle}{\left(\langle \Delta r_i^2 \rangle \cdot \langle \Delta r_j^2 \rangle \right)^{1/2}}$$

where, i and j stands for ith or jth residue and Δr_i or Δr_j represents displacement vectors correspond to ith and jth residue. The cross correlation (C_{ij}) varies within a range of -1 to $+1$ with lower and upper-limit indicates a fully anti-correlated and correlated motion during simulation time. In this instance, the DCC calculations were carried out taking into account the backbone Cα atomic fluctuations.

Principle component analysis

Principle component analysis is widely used in recent years to reduce dimensionality of data obtained from molecular dynamics simulations to extract dominant modes responsible for conformational (6). PCA was performed on C-alpha atoms using PTRAJ and CPPTRAJ modules (38) integrated with Amber 12. The data were averaged over 1000 snapshots with an equal interval of 100 ps in both cases. The first two principal components correspond to first two Eigen vectors of the covariance matrix (6). The scatter plot showing the dominant conformational motion representative of each structure was created using Origin data analyses program. The porcupine plots corresponding to first two normal modes were created using ProDy interface (40) integrated with Normal Mode Wizard plug-in of VMD (39).

Results and discussion

Binding mode of B9 with HIV-Nef

The docked structure of inhibitor B9 inside the active site of HIV-Nef dimeric cleavage provided crucial information on ligand binding landscape inside the active site of HIV-Nef (Figure 3). It can be observed that $-NO_2$ group attached with the phenyl ring involved in the formation of two hydrogen bond interactions with Gln104 and Gln107 residues of one subunit of HIV-Nef dimer. Interestingly, compound B9 binds at the dimeric cleavage of HIV-Nef dimer possessing multiple common residues from both sub-units in its active site. The 2D interaction plot (Figure 4) highlighted the position of inhibitor B9 in the HIV-Nef dimeric cleavage and common active site residues from each dimeric subunit. The binding mode clearly shows the presence of a hydrophobic/aromatic moiety, which is involved in proper binding of inhibitor in the dimeric groove, consists of some major active site residues involved in dimer packing, e.g. Asp108, Pro122, Leu112. Figure 4 further highlights the position of pharmacophoric features, which are necessary for a proper binding of inhibitor within residues involved in dimer packing, e.g. Gln104, Asn126, Gln107. Future efforts to understand detailed pharmacophoric features in combination with a recently reported structure activity relationship study (41) may provide structural benchmark to develop novel small molecule inhibitors using a rational approach.

It is believed that binding of compound B9 in the HIV-Nef dimeric cleavage leads to inhibition of HIV-Nef dimerization. The docked structure of compound B9 was further used to obtain a dynamic insight into the mechanism of dimerization inhibition by an aid of long-range molecular dynamics simulation.

MD simulations and post-dynamics analysis

RMSD, RMSF and radius of gyration

Figure 5 highlights the time-dependent root mean square deviation of backbone C-alpha atoms for both HIV-Nef free and ligand (B9) bound conformation. It was noticed that the backbone of both systems were well stabilized after a 30 ns time period. However, a larger magnitude (~2 Å) of fluctuation was observed in case of unbound conformation of HIV-Nef when compared with bound state. One possible

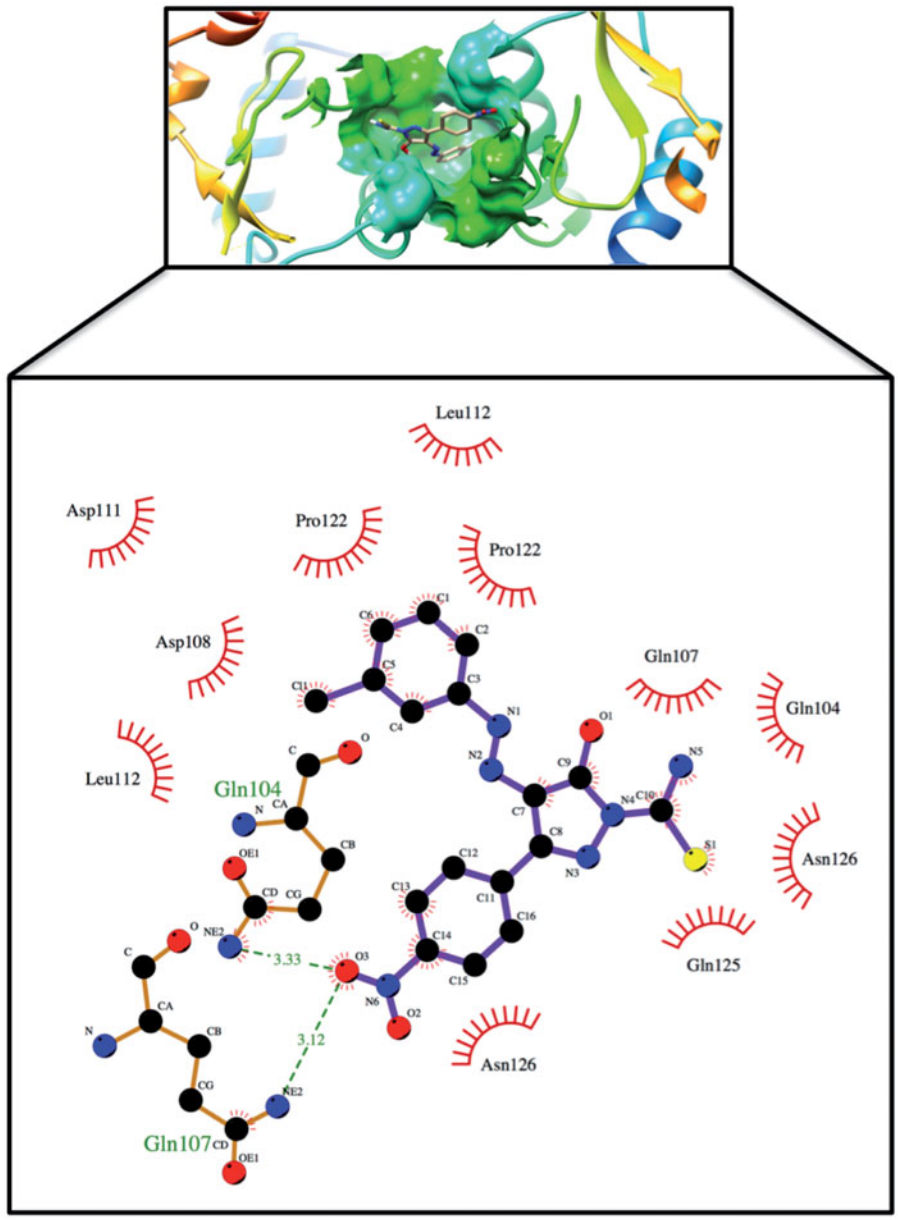

Figure 3. Residue interaction plot of compound, B9 inside the active site of HIV-Nef. Green dotted lines denote hydrogen bond interactions.

explanation of this phenomenon is that the attachment of inhibitor molecules inside HIV-Nef active site leads to a conformational rigidity, which hampers conformational evolution of HIV-Nef, especially during the process of dimerization.

To assess the effect of inhibitor (B9) binding on the conformational flexibility of the HIV-Nef, per-residue RMSF of C-alpha carbons were computed for both ligand-bound and apo conformations. From per-residue fluctuation (Figure 6) it can be clearly noticed that the presence of inhibitor inside the active site of HIV-Nef highly affected the conformational flexibility of the overall protein structure, which reflects the inhibition of dimerization in the presence of inhibitor. The significant difference (~2 Å) in average per-residue fluctuation clearly indicates a conformationally flexible nature of apo conformation, which might account for the disruption in dimerization. Furthermore, a more flexible region was observed between residues 138–152, which are located in one of the dimeric helix section of Nef (apo conformation). The higher value in RMSF might be due to the process of dimerization, which involves flexible helical residues located at Nef dimers. Whereas, the presence of B9 in the helical region inhibits the process of dimerization that affects the overall RMSF of Nef-B9 complex, as highlighted by lower average RMSF as well as lower magnitude of per-residue fluctuation at the helical region.

The overall fluctuations in RMSF further correlate with C-alpha RMSD fluctuations, which confirm a larger overall fluctuation in case of free conformation when compared with ligand-bound conformation of HIV-Nef. Figure 7 highlights the deviation of C-alpha residues located at the helical region of HIV-Nef active site, which clearly indicates more flexible nature of residues in unliganded (apo) HIV-Nef system when compared with bound conformation. The apo conformation showed a higher value of C-alpha deviations at the Nef helical region with an average RMSD of 5.17 Å, whereas its B9 counterpart displayed a comparatively lesser deviation with an average RMSD of 3.71 Å. This significant difference in

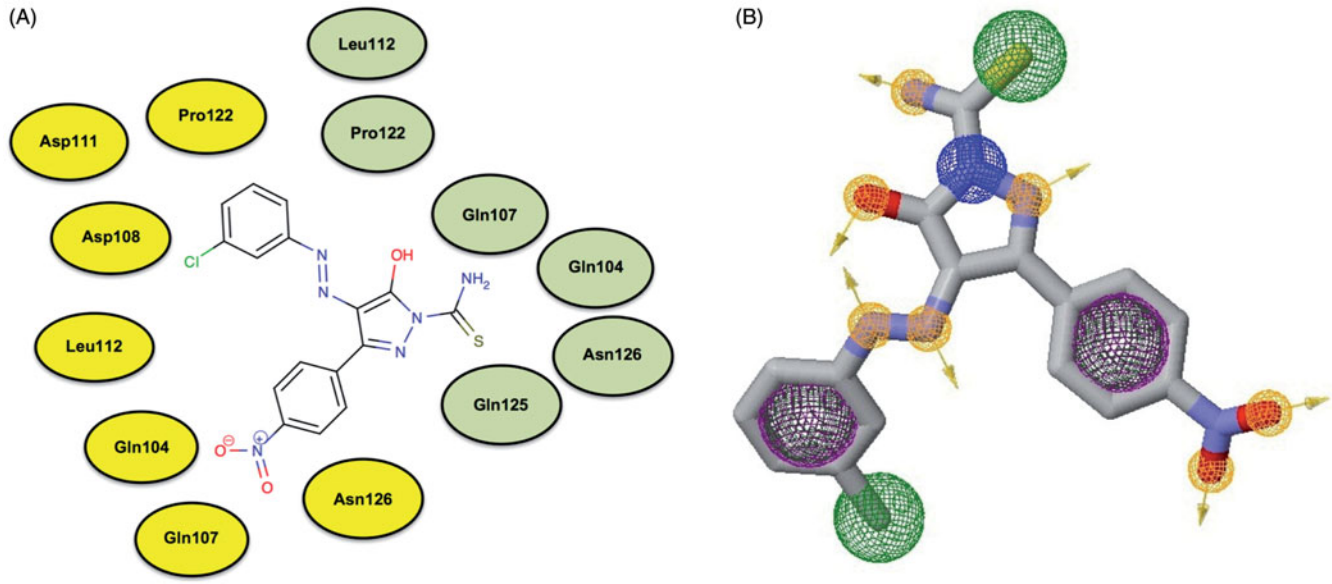

Figure 4. (A) 2D interaction map of compound B9 at the dimeric cleavage of HIV-Nef. Yellow and light green indicates the location of residues in each helical subunit. (B) Pharmacophoric feature of target bound conformation of compound B9.

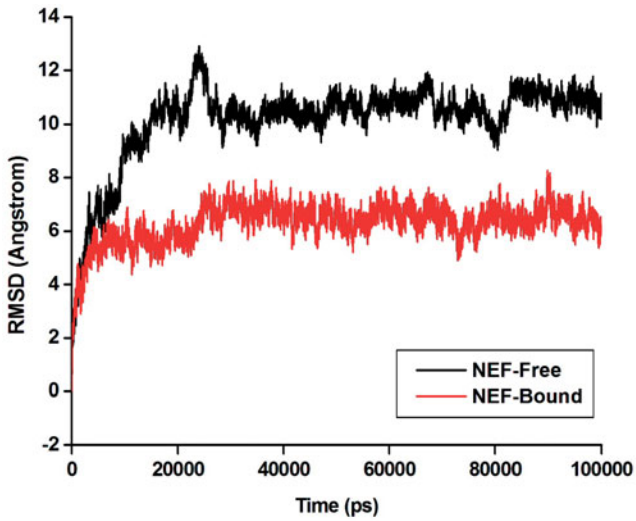

Figure 5. C-alpha backbone RMSD for HIV-Nef free and ligand bound conformations. The average C-alpha RMSD found to be 5.18 Å and 3.72 Å, respectively, for apo and B9 bound complex of HIV-Nef.

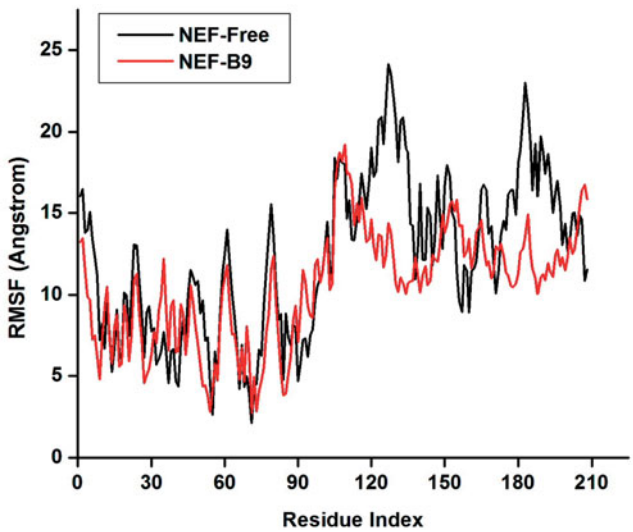

Figure 6. Residue-based fluctuation of HIV-Nef free and inhibitor bound conformation of HIV-Nef during the simulation time. The average C-alpha per-residue fluctuation for apo and bound conformations were found to be 12.26 and 10.48 Å, respectively.

C-alpha RMSD's (~2 Å) between helical region of native apo and bound conformations further highlights the helical flexibility, which played a significant role in the process of dimerization. Thus, it can be further postulated that attachment of inhibitor B9 in the helically active site of HIV-Nef leads to conformational rigidity, consequently impairs dimerization process.

These findings were further supported by the findings observed from the radius of gyration (Rg) (Figure 8).

The shape and folding of Nef-bound and free conformations over the trajectory can be seen in terms of Rg. Throughout the simulation, the apo conformation of HIV-Nef showed comparatively higher Rg value as compared to B9-Nef complex. The native apo conformation displayed an average Rg of 20.64 Å, whereas B9-Nef complex displayed a significantly lower Rg fluctuation with an average value of 19.04 Å. This larger breathing in Rg (~1.5 Å) in case of native apo conformation highly correlates with per-residue fluctuations and RMSD outcomes which justified an increased biomolecular flexibility of apo structure as compared to bound one. Binding of inhibitor B9 in the dimeric cleavage of HIV-Nef and its negative effect on dimeric flexibility confirms its inhibitory mechanism by hampering the overall biomolecular flexibility and dimer packing.

Understanding HIV-Nef dimerization

To further understand the dynamics of dimerization process, the distance between the orthogonally opposed residues (10) in each dimeric subunit are monitored along the dynamic simulations. These residues are highlighted in Figure 9.

Figures 10–13 clearly suggests that in case of apo protein the distances between the orthogonal residues are

significantly less when compared with bound conformation of HIV-Nef. Snapshots along the pathway of molecular dynamics simulations for apo- and B9-bound conformations of HIV-Nef further justified a lack of dimerization in case of Nef-B9 complex (Figure 14). The average distances between C-alpha atoms of orthogonally opposed Leu112, Gln104 and Asp108 residues in case of B9-bound conformation of HIV-Nef found to be 11.24, 24.23, 17.32 and 32.38 Å, respectively. Whereas, in case of apo conformation, the magnitude of average

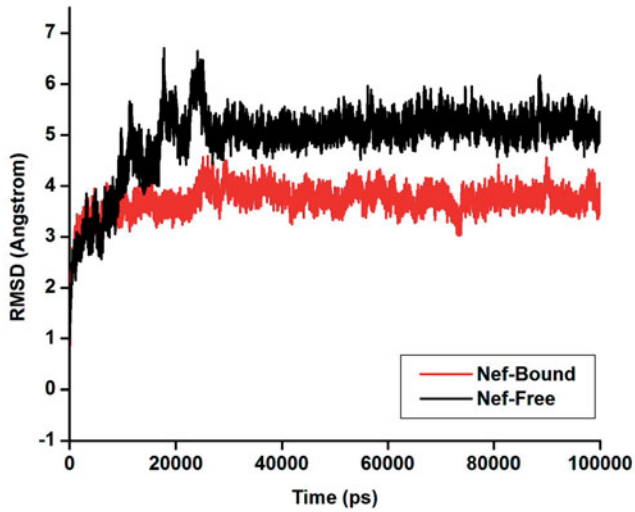

Figure 7. Deviation of C-alpha atoms of residues located at the active site helical region involved in the process of dimerization. The average RMSD's between apo and B9-Nef complex found to be 5.17 and 3.71 Å, respectively.

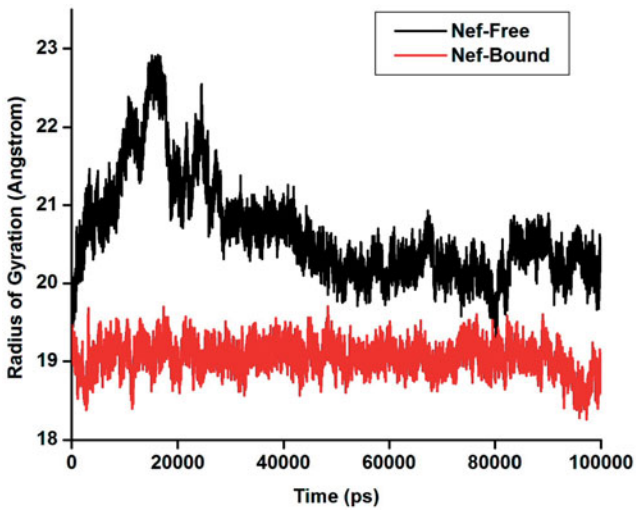

Figure 8. Radius of gyration of C-alpha atoms of HIV-Nef free and ligand-bound conformation. The average Rg of apo and bound conformations found to be 20.64 and 19.04 Å, respectively.

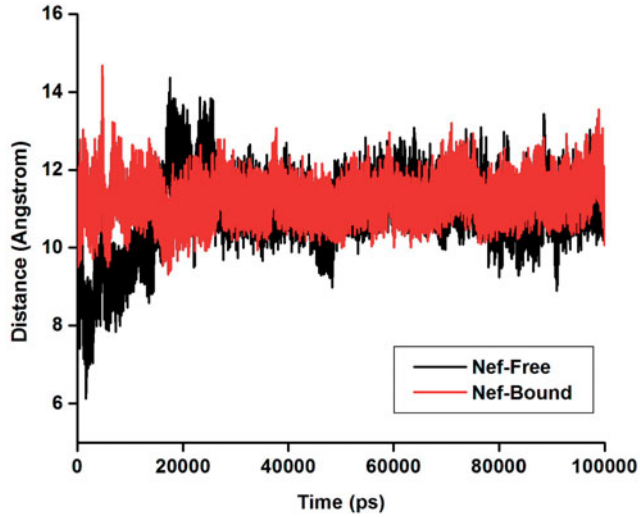

Figure 10. Distance between C-alpha residues involving Leu112 residues from both subunits. The average distance in case of apo conformation (10.93 Å) was lower as compared to bound conformation (11.24 Å).

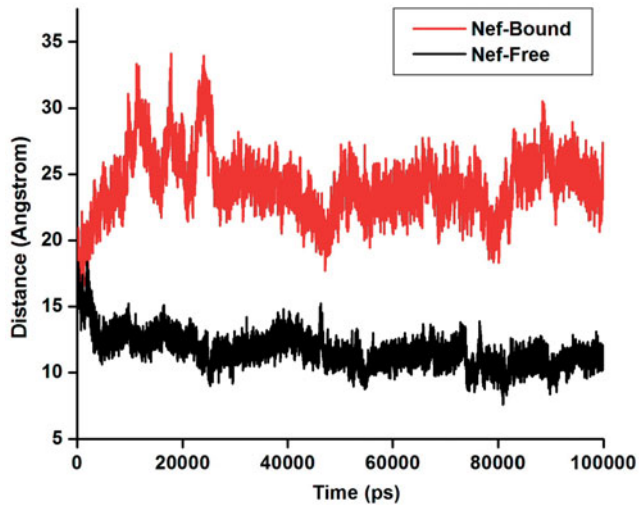

Figure 11. Distance between C-alpha residues involving Gln104's from both subunits. The average distances between two oppositely placed Gln104 residues were found to be 24.63 and 11.62 Å for B9-bound and apo conformation of Nef, respectively.

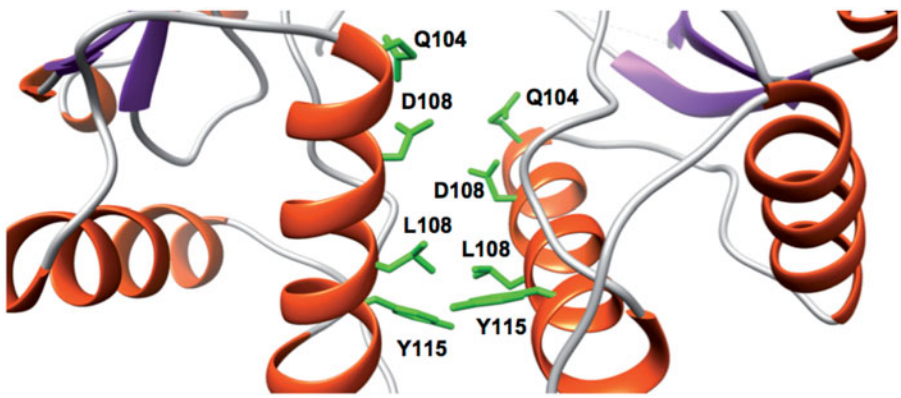

Figure 9. Position of orthogonally opposed residues at the dimeric helix of HIV-Nef believed to be involved in the process of dimerization (9,10).

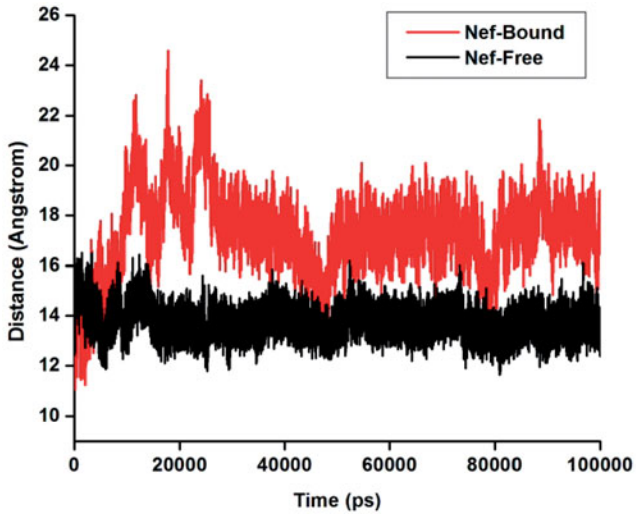

Figure 12. Distance between C-alpha residues involving Asp108 residues from both subunits. The average distances were 17.32 and 13.73 Å for bound and apo conformations of HIV-Nef, respectively.

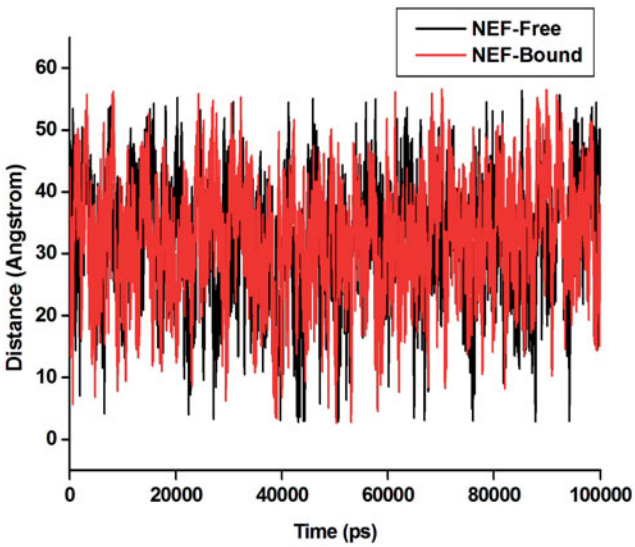

Figure 13. Distance between C-alpha residues involving Tyr115 residues from each monomer. The average distances were found to be 32.38 and 31.70 Å, respectively, for bound and apo conformations.

distances were comparatively less as the average C-alpha distances between Leu112, Gln104 and Asp108 found to be 10.93, 11.62 and 13.73 Å, respectively. These significant differences in distances among residues involved in dimer packing confirmed the lack of dimerization in Nef-B9 complex. This fact further co-relates with the experimental outcome, which confirmed a disruption of Nef dimerization by B9 using a cell-based assay (9).

The inhibition of dimer-dimer interaction as a result of B9 binding was further captured by an increase inter-residue distance between two oppositely placed Tyr115 residues (9) located at each dimer interface. The binding of B9 led to a ~1 Å increase in inter-residue contacts involving Tyr115 from each monomer (Figure 12). The occupancy of compound B9 inside the active site of HIV-Nef dimer was found responsible in increasing the average distances among residues (Table 2) involved in dimer packing, suggesting inhibition of HIV-Nef dimerization, which further substantiates the lack of conformational flexibility as a result of inhibitor binding.

Understanding the evolution of residues involved in dimer packing by analyzing the time-dependent snapshots of apo- and B9-bound conformation of Nef in combination with post-dynamics analysis, e.g. distance, Rg, RMSD, RMSF provides a model to understand the process of dimer packing and explains how the inhibitor gained access to the Nef dimeric site and its evolution in dimeric region leads to a dimeric inhibition. These outcomes from a classical molecular dynamics simulation unveils the large conformational drifts of HIV-Nef during the process of inhibitor binding, which will prove effective in designing novel Nef dimerization inhibitors.

Table 2. Residues involved in dimer packing (10) and their average distances from each other during simulation time.

Residues	Average distance (Å)	
Asp108-Asp108	17.32*	13.73
Leu112-Leu112	11.24*	10.93
Gln104-Gln104	24.23*	11.62
Tyr115-Tyr115	32.38*	31.70

*Denotes B9-bound conformation of HIV-Nef.

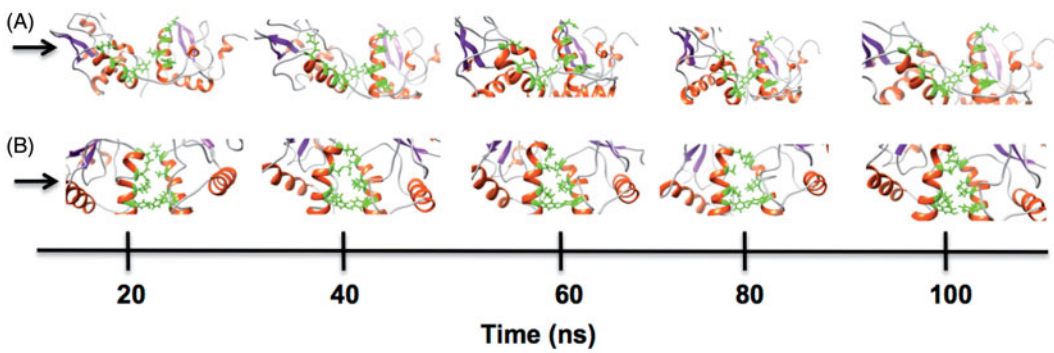

Figure 14. Snapshots of apo- and B9-bound conformations of HIV-Nef at a certain time interval during MD simulation. The residues highlighted in ''green'' are responsible in the process of dimer packing. A and B highlights the pathway of dimer dissociation and association for inhibitor (B9) bound and apo conformation, respectively.

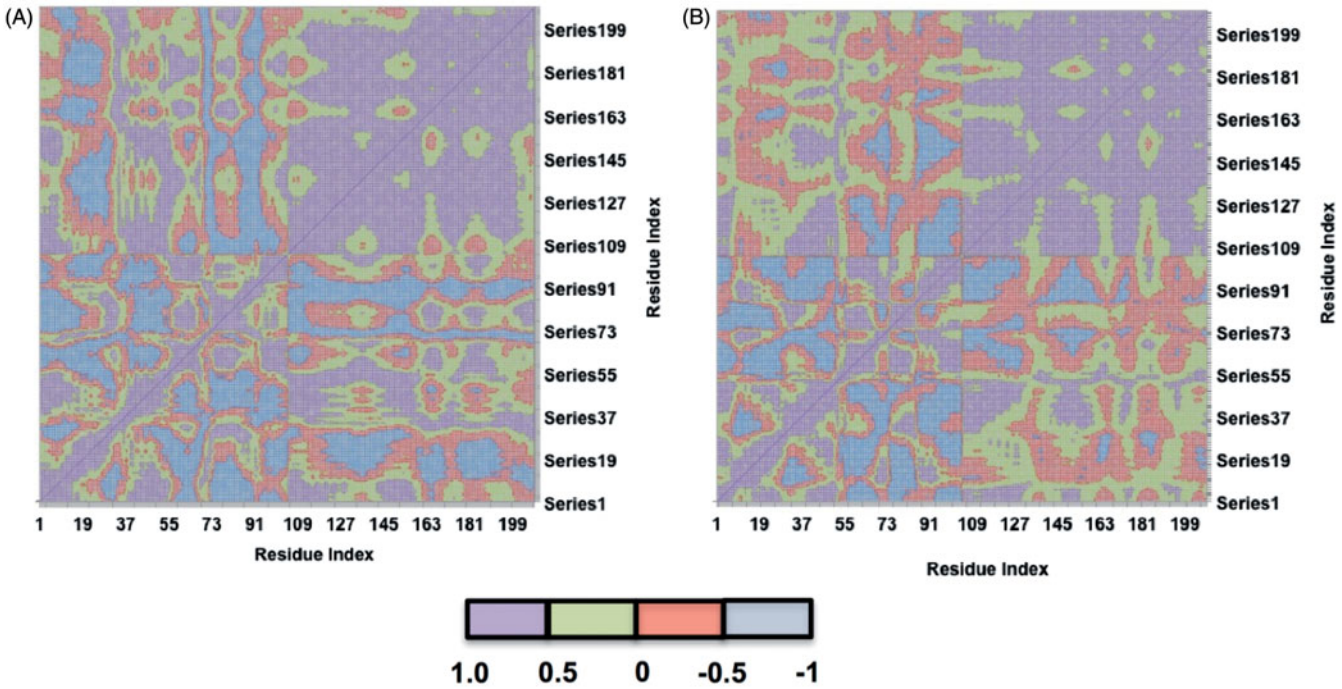

Figure 15. DCC map during simulation time taking in account Cα residues of HIV-Nef ligand-bound (A) and free (B) conformations.

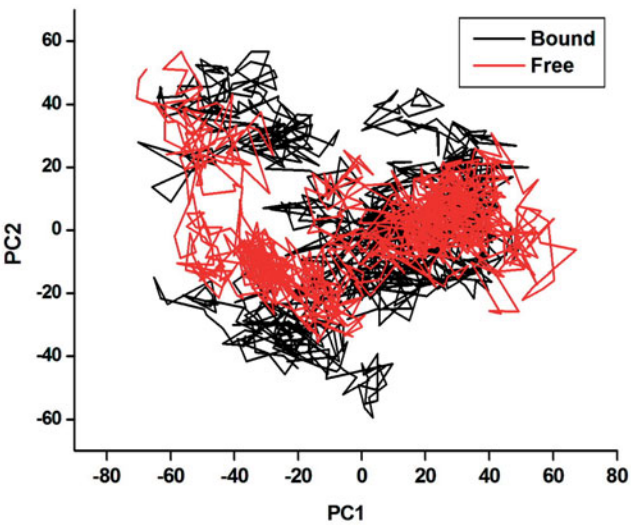

Figure 16. Projections of Eigen values during simulation period for ligand-bound and apo (free) conformations of HIV-Nef along the first two principal components (PC1 and PC2).

Dynamic cross-correlation analysis

Figure 15 highlights the cross-correlation map calculated for apo and bound conformation of HIV-Nef. It is evident from the correlation map that more globally correlated motion is observed in case of the free conformation of HIV-Nef, which further justifies the fact that in free conformation HIV-Nef went through a process of dimerization causing a more correlated residue-residue interaction. On the contrary, in case of bound conformation, a greater existence of negative correlated motions during simulation time was observed. This fact is further justified by observing a higher occupancy of positive C_{ij} patches in case of free conformation as compared to bound one. Such findings provide a solid conclusion on the mechanism of dimerization inhibition by B9.

Principal component analysis

To further understand conformational preferences for both ligand-bound and unbound conformations of HIV-Nef, PCA was carried out taking in account C-alpha residues of both the systems. Figure 16 highlights the dominant changes in motion across two principal components in the case of ligand-bound and unbound configurations of HIV-Nef. It was found that eigenvectors computed from individual trajectories were quite varied between the two systems, which further emphasize on the difference in the conformational landscape between the free and ligand-bound conformation. The difference in magnitude of Eigen values coming from first principal components of both apo and bound conformations was found to be ~0.05 Å whereas this difference was ~0.02 Å in case of the second principal component. This difference in average Eigen values across first two principal components suggests a greater mobility of the apo conformation as compared to its inhibitor-bound counterpart.

Moreover, porcupine plots across two normal modes clearly indicate a closer distance between helical dimers in free conformation when compared with B9-bound conformation of HIV-Nef (Figures 17 and 18). Also it clearly indicates an overall change in the direction of motion between bound and unbound conformation of HIV-Nef.

We also opted to monitor residue-based biomolecular flexibility across different normal modes in order to further understand the conformational flexibility and rigidity of the two systems, free and bound protein (Figures 19 and 20).

Interestingly, it was noticed that the flexibility of the residues ranging from 100 to 120 were comparatively higher

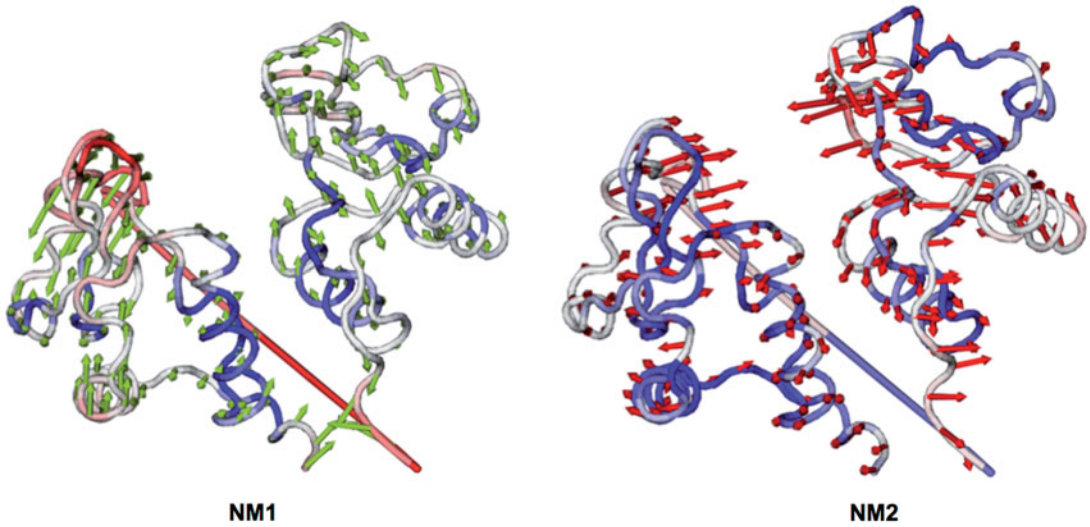

Figure 17. Porcupine plots across two different normal modes showing the direction of motion of unliganded (free) HIV-Nef system.

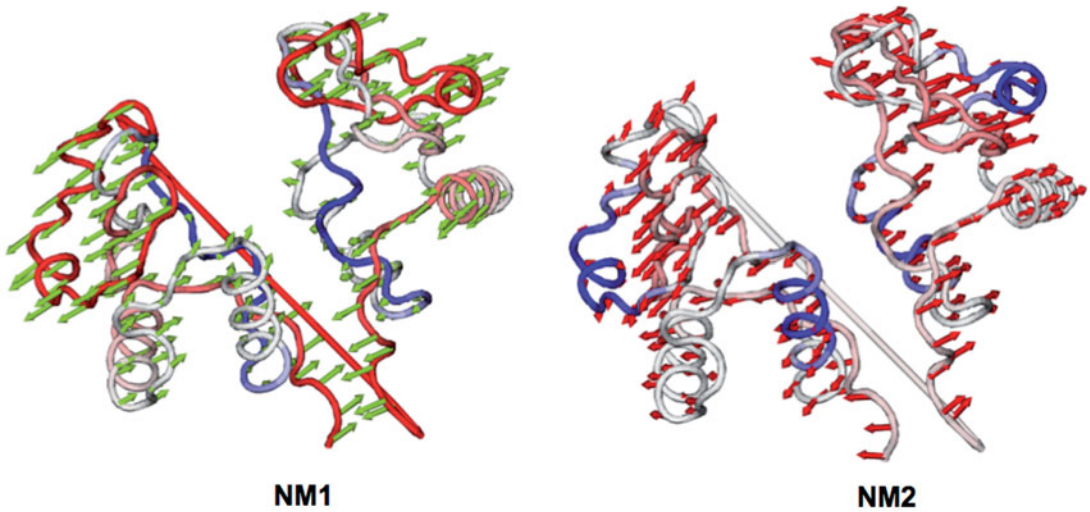

Figure 18. Porcupine plots across two different normal modes showing the direction of motion of ligand-bound (B9) HIV-Nef system.

in the case of apo conformation of HIV-Nef across first two normal modes. The average difference in fluctuation between apo- and B9-bound conformation of HIV-Nef within residues 138-152 found to be ~46.15 Å (mode 1) and ~0.60 Å (mode 2), respectively (Figures 19 and 20). This region contained residues involved in dimer packing. Normal mode analysis not only highlights the fact that the process of dimer packing affects the overall flexibility but also substantiates the findings of RMSD, Rg and RMSF parameters and further justifies the process of dimerization and its impact on overall protein flexibility.

Conclusion

Molecular dynamics simulation reveals a dimer packing and unpacking phenomena of HIV-Nef in its apo- and inhibitor-bound conformations. Small molecule inhibitors, such as B9, which targets the dimeric helical area of HIV-Nef, inhibits the process of dimerization thus leading to a more conformationally rigid system with hampered dimerization process. The RMSF, Rg and mobility plots generated during normal mode analysis for both the systems suggested a more conformational flexible nature of HIV-Nef dimer in the absence of an inhibitor. The increased magnitude of parameters, e.g. Rg (~1.5 Å), C-alpha deviations at the dimeric helix (~2 Å) suggested a greater conformational flexibility of Nef apo conformation and a flexible dimeric helix. On the contrary, B9-bound conformation of HIV-Nef was found to be more conformationally rigid with a lesser inter-dimeric association during the simulation period. Location of inhibitor, B9 in the active site of two helical subunits act as barrier in the process of dimerization, which can be easily understood by monitoring the distance among residues involved in the process of dimerization and as well as by visual inspection of snapshots generated during the long-range molecular dynamics simulation. The difference in magnitude of the distance parameter for inter-residue connection among Asp108, Leu112 and Gln104 was found to be 4, 1 and 12 Å, respectively. This first account report highlights important dynamic features of an important HIV target, which would

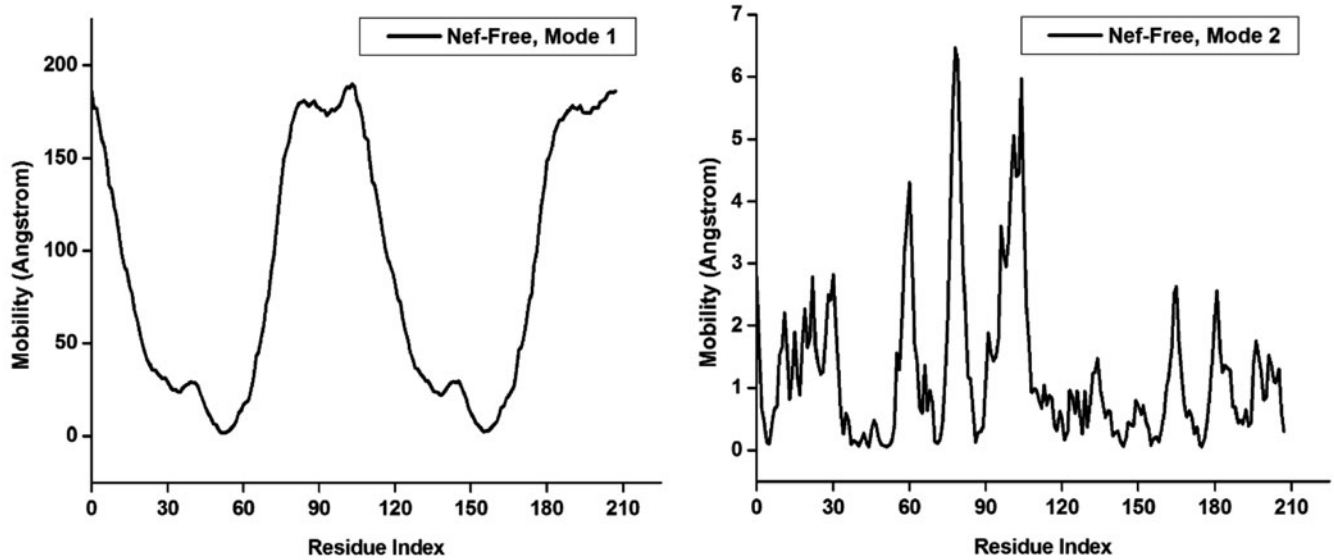

Figure 19. Comparison of mobility plot across first two normal modes (Mode 1 and 2) for apo conformation of HIV-Nef.

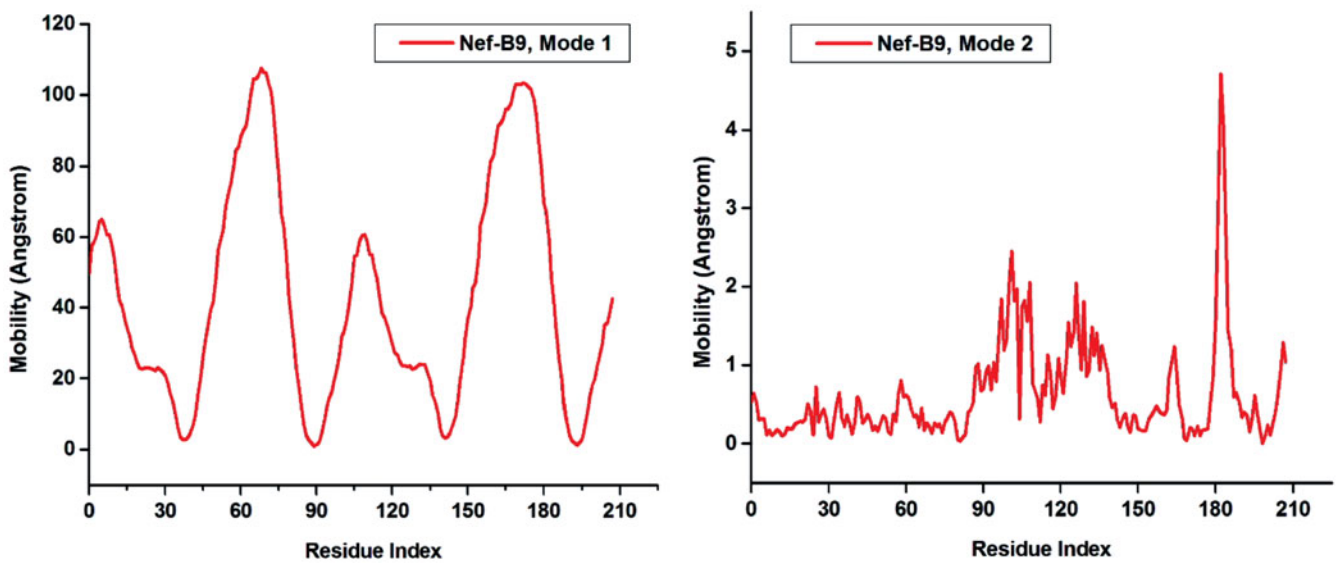

Figure 20. Comparison of mobility plot across first two normal modes (Mode 1 and 2) for B9-bound conformation of HIV-Nef.

also serve as an initial point in the process of designing novel compounds against HIV-Nef as anti-HIV drugs.

Acknowledgements

Authors acknowledge CHPC, Capetown, RSA, for high performance computational resources. SB acknowledges Open Source Drug Design and In Silico Molecules (OSDD-ISM) for technical support and useful discussions.

Declaration of interest

Authors declare no financial and intellectual conflict of interests.

SM, SB and MES acknowledge School of Health Sciences, University of KwaZulu-Natal, Westville, for financial support.

References

1. Rambaut A, Posada D, Crandall KA, Holmes EC. The causes and consequences of HIV evolution. Nat Rev Genet 2004;5:52–61.
2. Xu Y, Liu H, Niu CY, et al. Molecular docking and 3D QSAR studies on 1-amino-2-phenyl-4-(piperidin-1-yl)-butanes based on the structural modeling of human CCR5 receptor. Bioorg Med Chem 2004;12:6193–208.
3. Soliman MES. A hybrid structure/pharmacophore-based virtual screening approach to design potential leads: a computer-aided design of South African HIV-1 subtype C protease inhibitors. Drug Dev Res 2013;74:283–95.
4. Johnson BC, Pauly GT, Rai G, et al. A comparison of the ability of rilpivirine (TMC278) and selected analogues to inhibit clinically relevant HIV-1 reverse transcriptase mutants. Retrovirology 2012; 9:99.
5. Morah EU. Are people aware of their HIV-positive status responsible for driving the epidemic in SubSaharan Africa? The case of Malawi. Development Policy Review 2007;25:215–42.

6. Bhakat S, Martin AJM, Soliman MES. An integrated molecular dynamics, principal component analysis and residue interaction network approach reveals the impact of M184V mutation on HIV reverse transcriptase resistance to lamivudine. Mol Biosyst 2014; 10:2215–28.
7. Sarafianos SG, Das K, Hughes SH, Arnold E. Taking aim at a moving target: designing drugs to inhibit drug-resistant HIV-1 reverse transcriptases. Curr Opin Struct Biol 2004;14:716–30.
8. Das SR, Jameel S. Biology of the HIV Nef protein. Indian J Med Res 2005;121:315–32.
9. Emert-Sedlak LA, Narute P, Shu ST, et al. Effector kinase coupling enables high-throughput screens for direct HIV-1 Nef antagonists with antiretroviral activity. Chem Biol 2013;20:82–91.
10. Breuer S, Schievink SI, Schulte A, et al. Molecular design, functional characterization and structural basis of a protein inhibitor against the HIV-1 pathogenicity factor Nef. PLos One 2011;6: e20033.
11. Lindorff-Larsen K, Piana S, Dror RO, Shaw DE. How fast-folding proteins fold. Science 2011;334:517–20.
12. Garcia AE. Molecular dynamics simulations of protein folding. Methods Mol Biol (Clifton, N.J.) 2008;413:315–30.
13. Gsponer J, Caflisch A. Molecular dynamics simulations of protein folding from the transition state. Proc Natl Acad Sci USA 2002;99: 6719–24.
14. Swope WC, Pitera JW, Suits F, et al. Describing protein folding kinetics by molecular dynamics simulations. 2. Example applications to alanine dipeptide and beta-hairpin peptide. J Phys Chem B 2004;108:6582–94.
15. Durrant JD, McCammon JA. Molecular dynamics simulations and drug discovery. BMC Biol 2011;9:71–79.
16. Wan H, Hu J-p, Tian X-h, Chang S. Molecular dynamics simulations of wild type and mutants of human complement receptor 2 complexed with C3d. Phys Chem Chem Phys 2013;15: 1241–51.
17. Karubiu W, Bhakat S, Soliman MS. Compensatory role of double mutation N348I/M184V on nevirapine binding landscape: insight from molecular dynamics simulation. Protein J 2014;33:432–446.
18. Ruiz-Pernía JJ, Silla E, Tuñón I. Enzymatic effects on reactant and transition states. The case of chalcone isomerase. J Am Chem Soc 2007;129:9117–24.
19. Ruiz-Pernía JJ, Silla E, Tuñón I, Martí S. Hybrid quantum mechanics/molecular mechanics simulations with two-dimensional interpolated corrections: application to enzymatic processes. J Phys Chem B 2006;110:17663–70.
20. Thorpe IF, Brooks III CL. Conformational substates modulate hydride transfer in dihydrofolate reductase. J Am Chem Soc 2005; 127:12997–3006.
21. Zhang Y, Kua J, McCammon JA. Role of the catalytic triad and oxyanion hole in acetylcholinesterase catalysis: an ab initio QM/MM study. J Am Chem Soc 2002;124:10572–7.
22. Bruice TC, Bruice PY. Covalent intermediates and enzyme proficiency. J Am Chem Soc 2005;127:12478–9.
23. Benkovic SJ, Hammes-Schiffer S. A perspective on enzyme catalysis. Science 2003;301:1196–202.
24. Warshel A. Energetics of enzyme catalysis. Proc Natl Acad Sci 1978;75:5250–4.
25. Borodin O, Smith GD. Molecular dynamics simulations of poly(ethylene oxide)/LiI melts. 2. Dynamic properties. Macromolecules 2000;33:2273–83.
26. Falconi M, Biocca S, Novelli G, Desideri A. Molecular dynamics simulation of human LOX-1 provides an explanation for the lack of OxLDL binding to the Trp150Ala mutant. BMC Struct Biol 2007; 7:73–83.
27. Lee CH, Saksela K, Mirza UA, et al. Crystal structure of the conserved core of HIV-1 Nef complexed with a Src family SH3 domain. Cell 1996;85:931–42.
28. Pettersen EF, Goddard TD, Huang CC, et al. UCSF chimera - a visualization system for exploratory research and analysis. J Comput Chem 2004;25:1605–12.
29. Moonsamy S, Soliman MES. Dual acting HIV inhibitors: integrated rational in silico design strategy. Med Chem Res 2014;23:682–9.
30. Moonsamy S, Soliman MES. Computer-aided perspective for the design of flexible HIV non-nucleoside reverse transcriptase inhibitors (NNRTIs): de-novo drug design, virtual screening and molecular dynamics simulations. Lett Drug Design Discov 2014; 11:513–24.
31. Trott O, Olson AJ. Software news and update Autodock Vina: improving the speed and accuracy of docking with a new scoring function, efficient optimization, and multithreading. J Comput Chem 2010;31:455–61.
32. Lau CD, Levesque MJ, Chien S, et al. ViewDock TDW: high-throughput visualization of virtual screening results. Bioinformatics 2010;26:1915–17.
33. Goetz AW, Williamson MJ, Xu D, et al. Routine microsecond molecular dynamics simulations with AMBER on GPUs. 1. Generalized born. J Chem Theory Comput 2012;8:1542–55.
34. Wang JM, Wolf RM, Caldwell JW, et al. Development and testing of a general amber force field. J Comput Chem 2004;25:1157–74.
35. Lindorff-Larsen K, Piana S, Palmo K, et al. Improved side-chain torsion potentials for the Amber ff99SB protein force field. Proteins: Struct Funct Bioinf 2010;78:1950–8.
36. Jorgensen WL, Chandrasekhar J, Madura JD, et al. Comparsion of simple potential functions for simulating liquid water. J Chem Phys 1983;79:926–35.
37. Harvey MJ, De Fabritiis G. An implementation of the smooth particle mesh ewald method on gpu hardware. J Chem Theory Comput 2009;5:2371–7.
38. Roe DR, Cheatham III TE. PTRAJ and CPPTRAJ: software for processing and analysis of molecular dynamics trajectory data. J Chem Theory Comput 2013;9:3084–95.
39. Humphrey W, Dalke A, Schulten K. VMD: visual molecular dynamics. J Molec Graph Model 1996;14:33–8.
40. Bakan A, Meireles LM, Bahar I. ProDy: protein dynamics inferred from theory and experiments. Bioinformatics 2011;27:1575–7.
41. Iyer PC, Zhao J, Emert-Sedlak LA, et al. Synthesis and structure-activity analysis of diphenylpyrazolodiazene inhibitors of the HIV-1 Nef virulence factor. Bioorg Med Chem Lett 2014;24:1702–6.

Supplementary material available online